# Thermally-Induced Order−Order Transition of DNA−Cationic Surfactant Complexes

Wei-Long Hsu,[†] Yen-Cheng Li,[‡] Hsin-Lung Chen,*[,†] Willisa Liou,[§] U-Ser Jeng,[||] Hsien-Kuang Lin,[⊥] Wen-Liang Liu,[⊥] and Chain-Shu Hsu[‡]

*Department of Chemical Engineering, National Tsing Hua University, Hsin-Chu 30013, Taiwan, Department of Applied Chemistry, National Chiao Tung University, Hsin-Chu 30050, Taiwan, Department of Anatomy, Chang Gung University, Kwei-San, Taoyuan 333, Taiwan, National Synchrotron Radiation Research Center, Hsin-Chu 300, Taiwan, and Material and Chemical Research Laboratories, Industrial Technology Research Institute, Chutung, Hsinchu 310, Taiwan*

*Received March 31, 2006. In Final Form: June 8, 2006*

Polyanionic DNA interacts with cationic amphiphiles to form electrostatic complexes exhibiting rich self-assembled structures. This type of complex has been considered as a nonviral carrier in gene therapy and as a template for nanostructure construction. Here we report a thermally-induced phase transition of the complexes of DNA with the mixtures of a cationic surfactant, dodecyltrimethyl bromide (DTAB), and a neutral lipid, dioleoylphosphatidylethanolamine (DOPE), in fully hydrated state. An order−order transition between a multilamellar ($L_\alpha^c$) phase and an inverted hexagonal ($H_{II}^c$) phase was found to occur with the transition temperature adjustable by the DTAB-to-DNA base pair molar ratio ($x$) and DOPE-to-DTAB molar ratio ($m$). The stability of the $L_\alpha^c$ phase was enhanced at lower $m$ and $x$, as the $L_\alpha^c$-to-$H_{II}^c$ transition temperature increased with the decreases of these two parameters. The suppression of $L_\alpha^c$-to-$H_{II}^c$ transition at lower $x$ was attributed to the lower entropic gain from the counterion release due to the presence of uncomplexed DNA in the bulk solution.

## Introduction

Complexes of polyanionic DNA with cationic amphiphiles (CA) have gained much attention due to their important applications not only in gene therapy but also in nanostructure templating.[1−10] The structures of the complexes of DNA with cationic lipid (CL) and surfactant (CS) in a fully hydrated state have been characterized in detail to establish the relationship between the supramolecular structure and gene transfection efficiency.[3,8,10,11] The most prevalent structures observed thus far include a condensed multilamellar phase ($L_\alpha^c$) and an inverted hexagonal columnar phase ($H_{II}^c$) in which DNA was contained within the CA tubes arranged in a hexagonal lattice.[4,10,12−16] It has been demonstrated that the $H_{II}^c$-forming complex exhibited a better binding with anionic vesicles than the $L_\alpha^c$-forming complex;[3,10,11] however, a definite structure-transfection efficiency relationship is yet to be identified.[15]

In addition to gene therapy application, DNA−CA complexes have been demonstrated to be useful materials for nanostructure templating[2,5] and precursors for preparing stretchable films with good mechanical, optical, and electrical properties.[6,7,9] For this aspect of application, CS would represent a more attractive complexing agent for DNA compared with CL due to its lower cost and wider availability. DNA−CS complexes are also expected to display more versatile phase behavior with respect to the perturbations in complex composition, temperature, and aqueous environment than DNA−CL complexes due to the weaker hydrophobicity of the CS tail. Among these experimental variables, changing the temperature is a simple approach for switching the structure; this type of thermotropic phase transition, however, has not been studied in detail for DNA−CS complexes.

The thermally-induced phase transitions of some DNA−CL complex system have been revealed at the isoelectric composition.[17−19] In the previous studies of the isoelectric complexes composed of DNA and the cationic liposomes formed by

* To whom correspondence should be addressed. E-mail: hslchen@mx.nthu.edu.tw.

[†] Department of Chemical Engineering, National Tsing Hua University.

[‡] Department of Applied Chemistry, National Chiao Tung University.

[§] Chang Gung University.

[||] National Synchrotron Radiation Research Center.

[⊥] Industrial Technology Research Institute.

(1) Lasic, D. D.; Strey, H.; Stuart, M. C. A.; Podgornik, R.; Frederik, P. M. *J. Am. Chem. Soc.* **1997**, *119*, 832.

(2) Liang, H.; Angelini, T. E.; Ho, J.; Braun, P. V.; Wong, G. C. L. *J. Am. Chem. Soc.* **2003**, *125*, 11786.

(3) Lin, A. J.; Slack, N. L.; Ahmad, A.; George, C. X.; Samuel, C. E.; Safinya, C. R. *Biophys. J.* **2003**, *84*, 3307.

(4) Rädler, J. O.; Koltover, I.; Salditt, T.; Safinya, C. R. *Science* **1997**, 275, 810.

(5) Liang, H.; Angelini, T. E.; Braun, P. V.; Wong, G. C. L. *J. Am. Chem. Soc.* **2004**, *126*, 14157.

(6) Nakayama, H.; Ohno, H.; Okahata, Y. *Chem. Commun.* **2001**, 2300.

(7) Yang, C. Y.; Yang, W. J.; Moses, D.; Morse, D.; Heeger, A. J. *Synth. Met.* **2003**, *137*, 1459.

(8) Felgner, P. L.; Gadek, T. R.; Holm, M.; Roman, R.; Chan, H. W.; Wenz, M.; Northrop, J. P.; Ringold, G. M.; Danielsen, M. *Proc. Natl. Acad. Sci. U.S.A.* **1987**, *84*, 7413.

(9) Tanaka, K.; Okahata, Y. *J. Am. Chem. Soc.* **1996**, *118*, 10679.

(10) Koltover, I.; Salditt, T.; Rädler, J. O.; Safinya, C. R. *Science* **1998**, *281*, 78.

(11) Šmisterová, J.; Wagenaar, A.; Stuart, M. C. A.; Polushkin, E.; Brinke, G.; Hulst, R.; Engberts, J. B. F. N.; Hoekstra, D. *J. Biol. Chem.* **2001**, *276*, 47615.

(12) Dias, R. S.; Lindman, B.; Miguel, M. G. *J. Phys. Chem. B* **2002**, *106*, 12600.

(13) Gustafsson, J.; Arvidson, G.; Karlsson, G.; Almgren, M. *Biochim. Biophys. Acta* **1995**, *1235*, 305.

(14) Battersby, B. J.; Grimm, R.; Huebner, S.; Cevc, G. *Biochim. Biophys. Acta* **1998**, *1372*, 379.

(15) Congiu, A.; Pozzi, D.; Esposito, C.; Castellano, C.; Mossa, G. *Colloids Surf. B* **2004**, *36*, 43.

(16) Wu, C. M.; Liou, W.; Chen, H. L.; Lin, T. L.; Jeng, U. S. *Macromolecules* **2004**, *37*, 4974.

(17) Zantl, R.; Artzner, F.; Rapp, G.; Rädler, J. O. *Europhys. Lett.* **1998**, *45*, 90.

(18) Zantl, R.; Baicu, L.; Artzner, F.; Sprenger, I.; Rapp, G.; Rädler, J. O. *J. Phys. Chem. B* **1999**, *103*, 10300.

(19) Koynova, R.; MacDonald, R. C. *Biophys. J.* **2003**, *85*, 2449.

10.1021/la060862z CCC: $33.50 
Published on Web 08/02/2006

dimyristoylphosphatidylcholine (DMPC) and a neutral lipid (NL), dimyristoyltrimethylammonium propane (DMTAP), Zantl et al. have identified the transition between two distinct multilamellar phases, where a lamellar phase with gellike tails ($L_{\beta'}^c$) transformed to another with liquidlike tails ($L_\alpha^c$) at elevated temperature.[17,18] Koynova and MacDonald have disclosed the formations of temperature-dependent non-lamellar mesophases, such as $H_{II}^c$ phase and a bicontinuous $Q_{II}^c$ phases, using the isoelectric complexes of DNA with *o*-ethyldipalmitoylphosphatidylcholine (EDPPC) mixed with dielaidoylphosphoethanolamine (DEPE).[19] In the case of the DNA−CS complex, we recently reported a thermally-induced $L_\alpha^c$−$H_{II}^c$ phase transition in an isoelectric complex of DNA with dodecyltrimethyl bromide (DTAB) mixed with dioleoylphosphatidylethanolamine (DOPE). The complex with the DOPE-to-DTAB molar ratio (*m*) of 3 was found to exhibit $L_\alpha^c$ structure at room temperature; upon heating to 40 °C, the $L_\alpha^c$ phase transformed into the $H_{II}^c$ phase and the transition was thermally reversible in that the$L_\alpha^c$ structure was recovered upon cooling.

In the present study, we extend our previous work to systematically examine the effects of *m* and DTAB-to-DNA charge ratio on the $L_\alpha^c$−$H_{II}^c$ transition temperature for the DNA−(DTAB/DOPE) complex. First, we will revisit the self-assembled structures of the complexes at room temperature characterized by small-angle X-ray scattering (SAXS) to verify the containment of DNA in $L_\alpha^c$ and $H_{II}^c$ phases with the aid of electron density profile analysis. Then we will present a series of temperature-dependent SAXS profiles to reveal the transition between $L_\alpha^c$ and $H_{II}^c$ phase for the complexes with different charge ratios and *m*. It will be demonstrated that the $L_\alpha^c$-to-$H_{II}^c$ transition temperature depends significantly on these two parameters. The effect of charge ratio will be related to the entropic gain from the counterion release into the bulk solution containing the uncomplexed DNA.

## Experimental Sections

**Materials and Complex Preparation.** Linear DNA-type XIV from herring testes sodium salt (Na content 6.2%) was purchased from Sigma and used without further purification. Its molecular weight determined by gel electrophoresis was found to have a polydispersity value between 400 and 1000 base pairs (bp) with a center of distribution at ca. 700 bp.[20] DTAB and DOPE with purity of ca. 99% were obtained from Aldrich and Sigma, respectively, and were used without further purification.

The preweighed DTAB and DOPE were dissolved in chloroform followed by drying at room temperature to form a thin film. The film was hydrated by adding distilled water and then mixed by a vortex mixer for several minutes followed by sonicating in a cold water bath. DNA−(DTAB/DOPE) complexes were prepared by adding prescribed amount of 15 mg/mL DNA aqueous solution into the DTAB/DOPE suspension. The complexation resulted in visually identifiable precipitation. The complex suspensions were equilibrated at 4 °C before structural characterization. The adjustable composition parameters included the DOPE-to-DTAB molar ratio (denoted by *m*) and the charge ratio given by the DTAB-to-DNA base pair molar ratio (denoted by *x*) where $x = 2.0$ corresponded to the isoelectric composition for charge neutralization because each DTAB molecule has a positive charge and a base pair of DNA carries two negative charges. For the convenience of presentation, the complex with $x = i$ and $m = j$ will be abbreviated as *mix*j.

**Small-Angle X-ray Scattering (SAXS) Measurement.** The self-assembled structures of DNA−(DTAB/DOPE) complexes in the fully hydrated state were probed by SAXS. The aqueous suspensions of the complexes were directly introduced into the sample cell comprised of two Kapton windows. SAXS measurements were performed using a Bruker NanoSTAR SAXS instrument, which consisted of a Kristalloflex K760 1.5 kW X-ray generator (operated at 40 kV and 35 mA), cross-coupled Göbel mirrors for Cu Kα radiation ($\lambda = 1.54$ Å) resulting in a parallel beam of about 0.05 $mm^2$ in cross section at the sample position, and a Siemens multiwire type area detector with 1024 × 1024 resolution mode. The area scattering pattern has been radially averaged to increase the photon counting efficiency compared with the one-dimensional linear detector. The intensity profile was output as the plot of the scattering intensity ($I$) vs the scattering vector, $q = 4\pi/\lambda \sin(\theta/2)$ ($\theta$ = scattering angle). All scattering data were corrected by the empty beam scattering, the sensitivity of each pixel of the area detector, and thermal diffuse scattering ($I_{TDS}$). The thermal diffuse scattering was considered as a positive deviation from the Porod law[21,22] and may be associated with thermal motion, local disorder, or frozen-in fluctuations. $I_{TDS}$ can be regarded as a constant background, and the total scattered intensity in the high-$q$ region is expressed by the Porod−Ruland equation[21−23]

$$I(q) = \frac{K_p \exp(-\sigma^2 q^2)}{q^4} + I_{TDS} \quad (1)$$

where $K_p$ is the Porod's constant and $\sigma$ is a parameter related to the thickness of interphase for a two-phase structure. The exponential term in eq 1 becomes insignificant at sufficiently high $q$ such that a plot of $I(q)q^4$ vs $q^4$ would yield a straight line with a slope given by $I_{TDS}$. For the temperature-dependent measurement, the sample was first thermally equilibrated at the desired temperature for 30 min followed by data acquisition for 60 min.

**Transmission Electron Microscopy (TEM) Experiment.** TEM was used to examine the real-space morphology of DNA−(DTAB/DOPE) complexes. The specimens were prepared by a negative staining method which effectively vitrified the structure in the hydrated state.[24] A 5 μL drop of the solution was deposited onto a copper grid covered with carbon-coated Formvar film for 30 s. The specimen was then immediately stained for 30 s with 4% acidic uranyl acetate aqueous solution. The grid was blotted with the tip of a piece of filter paper and then air-dried for at least 3 h. The ultrathin specimens were examined on a JEOL 200EXII TEM operated at 100 kV.

**UV/Vis Measurements.** UV absorption spectra were recorded with a Hitachi U-3300 spectrophotometer to measure the concentration of DNA that remained in the supernatant upon complexation from the DNA absorption peak centering at 260 nm. Prior to the measurement, the separation between the supernatant and the precipitate was facilitated by centrifugation at a speed of 3200 rpm for 10 min. Quartz cells with an optical path of 1 cm were used for the spectroscopic measurements.

## Results and Discussion

**$L_\alpha^c$ and $H_{II}^c$ Phases of DNA−(DTAB/DOPE) Complexes at Room Temperature.** First, we present the self-assembled structures of the DNA−(DTAB/DOPE) complexes at room temperature (ca. 25 °C) probed by SAXS with detailed analysis of the electron density profiles. Figure 1a shows the room-temperature SAXS profile of the isoelectric *m*3*x*2 complex. This system exhibited four diffraction peaks with integral position ratio, which clearly indicated the formation of a multilamellar phase ($L_\alpha^c$) with the interlamellar distance ($d$) of 6.40 nm. Such a $L_\alpha^c$ phase with an in-plane ordering of the DNA chains confined in the hydrophilic layers has been considered as the predominant structure for DNA−CL complexes.[1,4,16,25] It is noted that the

(20) Dias, R.; Mel'nikov, S.; Lindman, B.; Miguel, M. G. *Langmuir* **2000**, *16*, 9577.
(21) Porod, G. *Kolloid-Z.* **1951**, *124*, 83.
(22) Porod, G. *Kolloid-Z.* **1952**, *125*, 51.
(23) Ruland, W. J. *J. Appl. Crystallogr.* **1971**, *4*, 70.
(24) Liou, W.; Geuze, H. J.; Slot, J. W. *Histochem. Cell Biol.* **1996**, *106*, 4.
(25) Hsu, W. L.; Chen, H. L.; Liou, W.; Lin, H. K.; Liu, W. L. *Langmuir* **2005**, *21*, 9426.

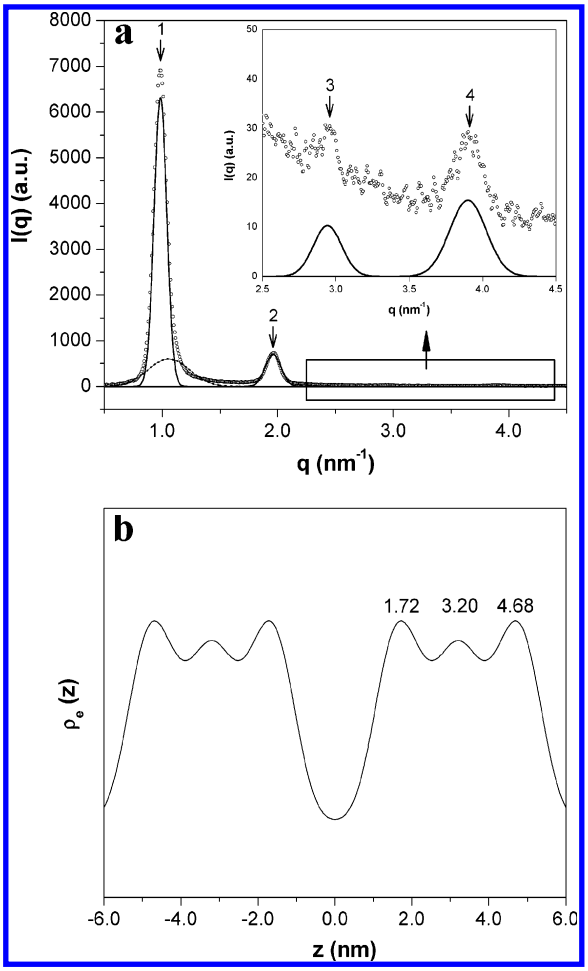


**Figure 1.** (a) SAXS profiles collected at room temperature for the isoelectric DNA−(DTAB/DOPE) complex ($x = 2$) with $m = 3$, showing the formation of $L_\alpha^c$ phase. The solid curves represent the fitting result of the scattering peaks using Gaussian function. The broad peak overlapped with the sharp primary lamellar peak is the DNA-DNA correction peak. The inset displays the third- and fourth-order lamellar peak. The third-order diffraction is apparently weaker than the fourth-order peak. (b) The electron density profile of the $L_\alpha^c$ phase calculated from the scattering pattern in panel a using eq 1. The two humps at $z = 1.72$ and 4.68 nm are associated with the headgroup regions, and the protrusion at 3.20 nm represents the DNA confined between the bilayers.

scattering peak, $q_{DNA}$, associated with the in-plane correlation of the DNA chains was not observed in the present system. We however believe that such a correlation did exist because the $q_{DNA}$ peak had been identified for other compositions.[25] Here, $q_{DNA}$ may have overlapped with the primary peak associated with the multilamellar structure due to a relatively large interhelical distance ($d_{DNA} = 2\pi/q_{DNA}$). It is also worth noting that the intensity of the third-order lamellar peak was apparently weaker than that of the fourth-order peak. As the intensity of the $n$th-order diffraction from the lamellar array is propotional to $\sin^2(n\pi f_w)$ with $f_w$ being the volume fraction of the hydrophilic layer,[26] the diminishment of the third-order peak means that the thickness of the hydrophobic bilayer ($d_L$) was approximately twice that of the hydrophilic layer ($d_w$). Therefore, the thickness of the hydrated DNA monolayer was estimated to be $d_w = d/3 = 2.14$ nm, which corresponded well to the diameter of B−DNA.

The electron density profile constructed from the SAXS data can also yield the quantitative values of $d_w$ and $d_L$ and verify the intercalation of DNA between the bilayers. The electron density profile along the lamellar normal (i.e., $z$ direction) in the $L_\alpha^c$ phase is given by[16,27]

$$\rho_e(z) \sim \sum_{k=1}^{n} F_k \cos(q_k z)\phi_k \sim \sum_{k=1}^{n} [I_k q_k^2]^{1/2} \cos(q_k z)\phi_k \quad (2)$$

where $n$ is the total number of diffraction order, $q_k$ is the scattering vector of the $k$th diffraction order, $I_k$ is the corresponding scattering intensity, $[I_k q_k^2]^{1/2}$ is the magnitude of the $k$th amplitude (i.e., $F_k$), and $\phi_k$ is the phase which is either $-1$ or $+1$ for a centrosymmetrical lamellar structure.[28] To obtain the correct intensity $I_k$ of the diffraction peak at $q_k$, fittings of the scattering curves by a series of Gaussian peaks were conducted [cf. Figure 1a], and $I_k$ and $q_k$ were identified as the height and position of the corresponding fitted Gaussian peak, respectively. The values of these two parameters thus obtained were then substituted into eq 2 to calculate the electron density profile.

Figure 1b presents the electron density profile obtained from the diffraction pattern in Figure 1a with the most reasonable phase combination of (- - -+). The humps with the same $\rho_e(z)$ at $z = \pm 1.72$ and $\pm 4.68$ nm represented the headgroup regions and a protrusion at $z = \pm 3.2$ nm corresponded to the DNA confined between the lipid bilayers. Considering the significantly different polarity between the hydrophilic and hydrophobic layers, the boundary between these two phases should be sharp, as has been verified for the complexes of synthetic polyelectrolytes with lipids.[29−31] In this case, the thickness of the hydrophilic layer was given by the distance between the two humps (intervened by the DNA peaks) representing the headgroups, which was 2.96 nm. The thickness of the hydrophobic layer was hence given by $d_L = d - d_w = 3.44$ nm. The observed $d_w$ closely agreed with that calculated from one-third of the interlamellar distance.

In addition to the $L_\alpha^c$ phase, the isoelectric DNA−(DTAB/DOPE) complex has been shown to display the $H_{II}^c$ phase at room temperature when the content of DOPE in the membrane was sufficiently high. Figure 2a shows the room-temperature SAXS profile of the $m9x2$ complex. A series of diffraction peaks with the relative positions of $1:3^{1/2}:4^{1/2}:7^{1/2}:9^{1/2}$... were observed, indicating the formation of a 2-D hexagonal lattice with the characteristic spacing of $d = 7.04$ nm.

The corrected intensity $I_{hk}$ associated with the ($h$ $k$) diffraction plane of a hexagonal lattice is related to its amplitude $F_{hk}$ by[28,32−35]

$$I_{hk} \approx k F_{hk}^2 / q_{hk} \quad (3)$$

where $k$ is a multiplicity factor with the value of 2 for (2 1), (3 1), (3 2), and (4 1) planes and 1 for other planes.[28] The electron density at any position ($y$, $z$) in the lattice is given by

$$\rho_e(y, z) \sim \sum F_{hk} \cos(q_{hk} y) \cos(q_{hk} z)\phi_{hk} \quad (4)$$

where $\phi_{hk}$ is a phase which is either $-1$ or $+1$ for the hexagonal

(26) Roe, R. J. *Methods of X-ray and Neutron Scattering in Polymer Science*; Oxford University Press: New York, 2000.
(27) Wachtel, E.; Borochov, N.; Bach, D.; Miller, I. R. *Chem. Phys. Lipids* **1998**, *92*, 127.
(28) Warren, B. E. *X-ray diffraction*; Addison-Wesley: Reading, MA, 1969.
(29) Antonietti, M.; Kaul, A.; Thünemann, A. *Langmuir* **1995**, *11*, 2633.
(30) Thünemann, A. F.; Lochhaas, K. H. *Langmuir* **1998**, *14*, 6220.
(31) Thünemann, A. F.; Beyermann, J. *Macromolecules* **2000**, *33*, 6878.
(32) Harper, P. E.; Mannock, D. A.; Lewis, R. N. A. H.; McElhaney, R. N.; Gruner, S. M. *Biophys. J.* **2001**, *81*, 2693.
(33) Turner, D. C.; Gruner, S. M. *Biochemistry* **1992**, *31*, 1340.
(34) Francescangeli, O.; Pisani, M.; Stanić, V.; Bruni, P.; Weiss, T. M. *Europhys. Lett.* **2004**, *67*, 669.
(35) Rappolt, M.; Hickel, A.; Bringezu, F.; Lohner, K. *Biophys. J.* **2003**, *84*, 3111.

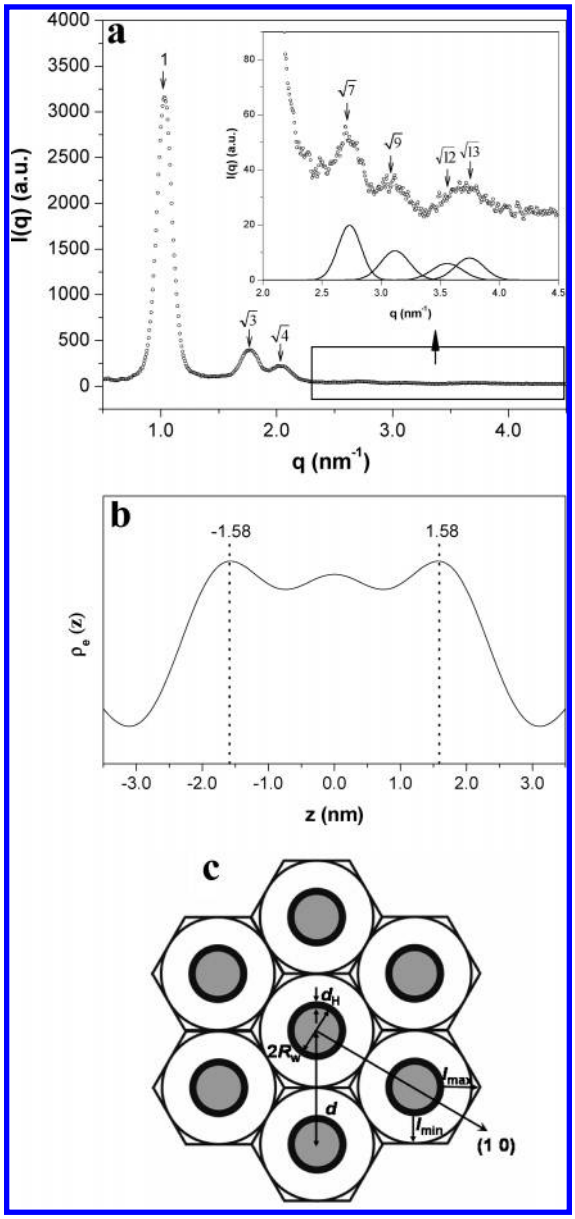


**Figure 2.** (a) SAXS profiles collected at room temperature for the isoelectric DNA−(DTAB/DOPE) complexes with $m = 9$, indicating the formation of $H_{II}^c$ phase. The inset shows the higher-order peaks. (b) The electron density profile along the (1 0) direction obtained from eq 3. The two humps at $z = \pm 1.58$ correspond to the two headgroups. (c) Schematic illustration of the cross-section of the $H_{II}^c$ phase.

structure.[28] The phase combination of (+- -++++) has been regarded as the most reasonable choice for the inverted hexagonal phase, as has been demonstrated for neat phosphatidyl−ethanolamine (PEs) in a fully hydrated state and the complex of DNA with DOPE in the presence of iron ions.[32−35] Here we also adopted this phasing choice to calculate the electron density profile along the normal to the (10) plane (corresponding to the case of $y = 0$). Figure 2b displays the electron density profile. The origin at the $z$ axis corresponded to the center of the tube containing DNA. Two hydrophobic valleys were found to locate at ±3.1 nm, and the two humps beside the valleys represented the two polar headgroups located at ±1.58 nm. Therefore, the nearest distance between two headgroups along the (1 0) direction, $d_{HH}$, is equal to 3.16 nm. We assumed that DOPE dominated the characteristic geometry of the $H_{II}^c$ structure because of large $m$; hence, the average headgroup thickness ($d_H$) was 0.77 nm as

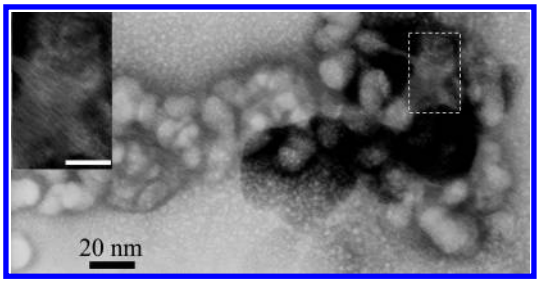


**Figure 3.** TEM micrograph showing the side-view image of the columnar structure formed by *m*9*x*2 complex. The inset shows the magnified image of the region enclosed by the dashed rectangle. The scale bar in the inset corresponds to 10 nm.

calculated from the headgroup area of 0.47 nm$^2$ assuming spherical shape.[36] The distance, $d_{HH}$, was equal to the sum of $d_H$ and the diameter of the water core, $2R_w$ (cf. Figure 2c). Hence, $2R_w$ was given by $d_{HH} - d_H = 2.39$ nm. This value agreed well with the reported diameter of hydrated B-DNA.[37] The maximum and minimum extension of the acyl chains in the Wigner-Seitz cell can be obtained by

$$2l_{min} = d - 2d_H - 2R_w \quad (5)$$

$$l_{max} = (d/3^{1/2}) - d_H - R_w \quad (6)$$

Taking $d = 7.04$ nm, $d_H = 0.77$ nm, and $2R_w = 2.39$ nm, $l_{min}$ and $l_{max}$ calculated by these two equations are 15.6 and 21.0 Å, respectively.

The formation of the $H_{II}^c$ phase was also verified by the TEM micrograph in Figure 3 showing the parallel strips corresponding to the side-view of the DNA-containing tubes. This morphological texture was distinguished from the fingerprint-like pattern observed for the $L_\alpha^c$ phase.[14,16,25]

In addition to the self-assembled structure, the secondary structure of DNA confined within the hydrophilic gallery was also identified by the X-ray scattering profile in the high-$q$ region recorded with a synchrotron radiation source (which enhanced the S/N ratio at high $q$) to reveal whether the electrostatic interaction with CS could perturb the duplex conformation. The use of an $I(q)$ vs $q$ plot to reveal the secondary structure of DNA has already been demonstrated two decades ago by Müller, who calculated the scattering patterns for DNA with A, B, and C conformations (cf. inset of Figure 4).[38] Therefore, the DNA conformation in the complexes may be disclosed conveniently by comparing the experimentally observed intensity profile with the calculated ones in the appropriate $q$ region. Figure 4 displays the scattering curves of *m*1*x*2 and *m*3*x*1 complexes in the $q$ range of 4.0−9.0 nm$^{-1}$. Both compositions were found to exhibit two broad peaks at ca. 4.9 and 7.4 nm$^{-1}$, with the former overlapping with the fifth-order diffraction peak associated with the multilamellar structure. Qualitatively, the observed scattering patterns agreed with that of B−DNA shown in the inset and differed significantly from the profiles of A and C conformations. The B conformation is the most common secondary structure of DNA in the fully hydrated state. Our X-ray scattering results suggested that B conformation of DNA still retained under the electrostatic interaction with the membrane.

The foregoing results have revealed a lyotropic phase transition for the DNA−(DTAB/DOPE) complex, where the $L_\alpha^c$ phase transformed into the $H_{II}^c$ phase at room temperature with the

(36) Tate, M. W.; Gruner, S. M. *Biochemistry* **1989**, *28*, 4245.
(37) Podgornik, R.; Rau, D. C.; Parsegian, V. A. *Macromolecules* **1989**, *22*, 1780.
(38) Müller, J. J. *J. Appl. Crystallogr.* **1983**, *16*, 74.

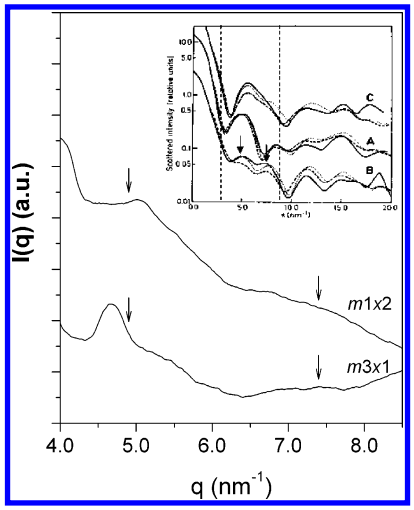


**Figure 4.** X-ray scattering profiles in the high-$q$ region of $m1x2$ and $m3x1$ complexes. Two broad peaks situating at 4.9 and 7.4 nm$^{-1}$ (marked by the arrows) are observed with the former overlapping with the fifth-order diffraction from the $L_\alpha^c$ phase. The inset displays the scattering curves of the three conformational forms (A, B, and C) of DNA calculated by Müller.[32] The observed scattering patterns agreed with that of B-DNA in the region enclosed by the dashed lines.

increase of the DOPE content in the membrane. In the following, we will discuss the thermotropic phase behavior of the complexes with the $L_\alpha^c-H_{II}^c$ transition induced by varying temperature. We will examine how $x$ and $m$ affect the transition temperature.

**Thermally-Induced $L_\alpha^c-H_{II}^c$ Order-Order Transition.** Figure 5 presents the temperature-dependent SAXS profiles of $m1x2$ and $m1x3$ complexes. These two systems exhibited the stable $L_\alpha^c$ phase as this structure persisted upon heating to as high as 70 °C. The interlamellar distance was found to decrease slightly with increasing temperature, and this trend was accompanied by a slight swelling of $d_{DNA}$. The reduction of $d$ may be attributed to the more coiled conformation of the alkyl tails at higher temperature due to the higher population of the bonds in the gauche conformational state. This decrease of $d$ caused an enlargement of the surface area of the lamellae, which then led to a swelling of $d_{DNA}$. A similar temperature effect on $d$ and $d_{DNA}$ has also been observed in the previous studies of the DNA−(DMTAP/DMPC) complex.[17,18] The DNA−DNA correlation peak became sharper when the complex was cooled back to 30 °C from 70 °C, indicating that the thermal annealing at elevated temperature could enhance the in-plane ordering of DNA within the hydrophilic gallery.

Figure 6a displays the temperature-dependent SAXS profiles of the $m2x2$ complex collected in a heating cycle. The system exhibited only the $L_\alpha^c$ phase before 58 °C. When the temperature was raised to 61 °C, a new set of scattering peaks with the relative positions of $1:3^{1/2}:4^{1/2}$ emerged, indicating of development of the $H_{II}^c$ phase. Upon further heating, the intensity of the $H_{II}^c$ diffraction peaks grew at the expense of the $L_\alpha^c$ peaks. The intensity of the primary $H_{II}^c$ peak [$I_m(H_{II}^c)$] was found to increase linearly with increasing temperature, as shown in Figure 6b which plots the corrected $I_m(H_{II}^c)$ against the absolute temperature. The temperature at which $I_m(H_{II}^c)$ became zero obtained through linear extrapolation was 54.7 °C. This temperature was considered as the onset temperature, $T_o$, of the $L_\alpha^c-H_{II}^c$ transition on heating. Table 1 lists the values of $T_o$ of other complex compositions obtained through such a linear extrapolation.

It can be seen from Table 1 that the onset of the $L_\alpha^c-H_{II}^c$ transition depended on both the membrane composition ($m$) and

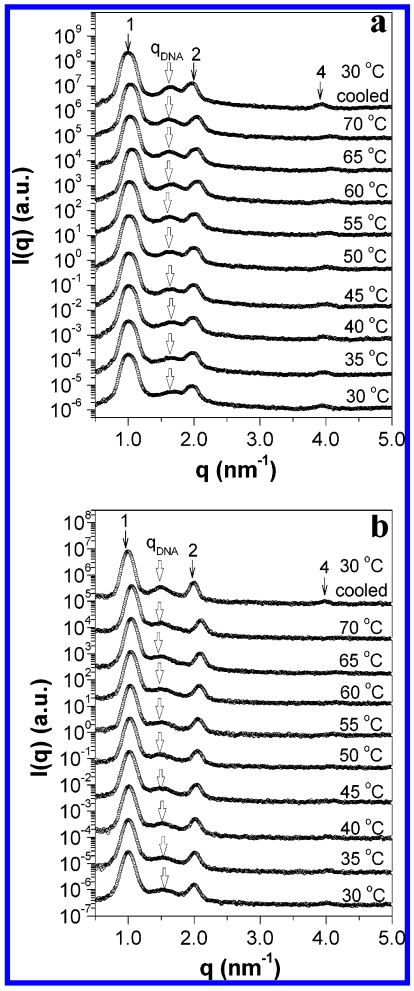


**Figure 5.** Temperature-dependent SAXS profiles of (a) $m1x2$ and (b) $m1x3$ complexes. Only the $L_\alpha^c$ phase was observed over the temperature range studied.

the DTAB-to-DNA base pair charge ratio ($x$), where $T_o$ decreased with the increases of these two parameters. It has been demonstrated that the $L_\alpha^c$ phase may transform into the $H_{II}^c$ phase lyotropically by adjusting the membrane composition to increase the membrane spontaneous curvature or by mediating the hydration environment to reduce the membrane rigidity.[10] The former is a common approach which may be accomplished by the addition of phoshpatidylethanolamine (PE) lipid, which by itself tends to form cylindrical micelles in aqueous media. The presence of PE lipid in the membrane mixture would invariably promote the propensity of the complex to form a columnar structure; consequently, the thermally-induced $L_\alpha^c-H_{II}^c$ transition not observable in the complexes with rather dilute DOPE concentration (e.g., $m = 1$) became accessible at $m \geq 2$, and the transition temperature decreased with further increase of $m$.

The $L_\alpha^c-H_{II}^c$ transition temperature was also influenced by $x$ under a given membrane composition, as the complex with larger $x$ was found to exhibit a lower $T_o$. This effect may be understood by considering the entropic gain from the release of counterions upon the phase transition, as schematically illustrated in Figure 7. Previous studies have shown that neutralization of the charges on DNA is less efficient in the $L_\alpha^c$ phase compared to the $H_{II}^c$ phase due to the mismatch in surface curvature between the planar cationic membrane and the DNA cylinder.[39,40] In this

(39) May, S.; Harries, D.; Ben-Shaul, A. *Biophys. J.* **2000**, *78*, 1681.
(40) Krishnaswamy, R.; Raghunathan, V. A.; Sood, A. K. *Phys. Rev. E* **2004**, *69*, 031905.

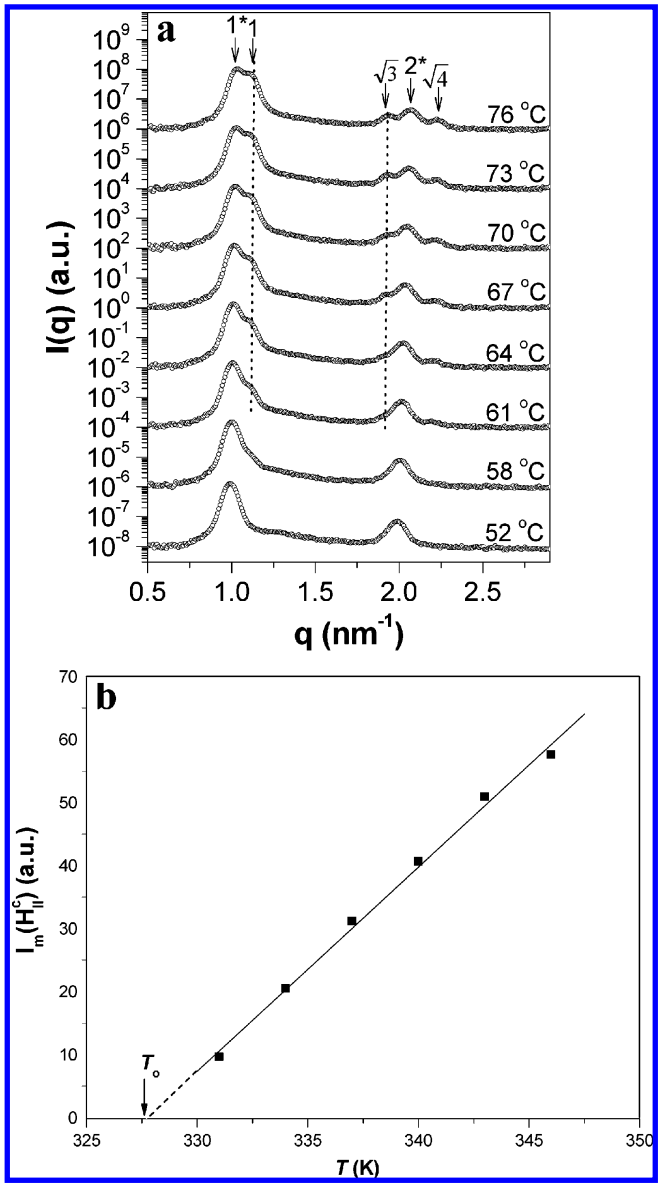


**Figure 6.** (a) Temperature-dependent SAXS profile of *m*2*x*2 complex revealing an order-order phase transition from $L_\alpha^c$ to $H_{II}^c$ phase on heating. (b) Plot of $I_m(H_{II}^c)$ vs $T$ to determine the onset temperature of $L_\alpha^c$-to-$H_{II}^c$ transition by a linear extrapolation to $I_m(H_{II}^c) = 0$.

**Table 1. Onset Transition Temperature ($T_o$) of $L_\alpha^c$-to-$H_{II}^c$ Transition for the Complexes with Different Compositions**

| composition | $T_o$ | composition | $T_o$ |
|---|---|---|---|
| *m*1*x*2 | n/a | *m*2*x*4.5 | 51.0 °C |
| *m*1*x*3 | n/a | *m*3*x*0.8 | 52.0 °C |
| *m*2*x*1 | n/a | *m*3*x*1 | 40.5 °C |
| *m*2*x*2 | 55.0 °C | *m*3*x*2 | 33.6 °C |
| *m*2*x*4 | 52.0 °C | | |

case, a portion of $Na^+$ counterions should remain condensed on the phosphate groups (located at the side along the in-plane direction of the bilayer) not bound with the CS. When the structure transforms into the $H_{II}^c$ phase, the DNA chains are wrapped around by the cationic membrane for effective charge matching; therefore, most of these counterions are released into the bulk solution, leading to an entropic gain. This entropic gain is however reduced if the bulk solution contains uncomplexed DNA, since the space available for the counterions to explore becomes smaller.[41] As a result, a higher uncomplexed DNA concentration

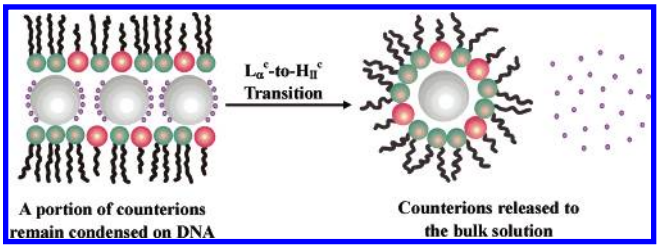


**Figure 7.** Schematic illustration showing the release of counterions upon the transition from the $L_\alpha^c$ phase to the $H_{II}^c$ phase because the negative charges on DNA are neutralized more effectively in the $H_{II}^c$ phase.

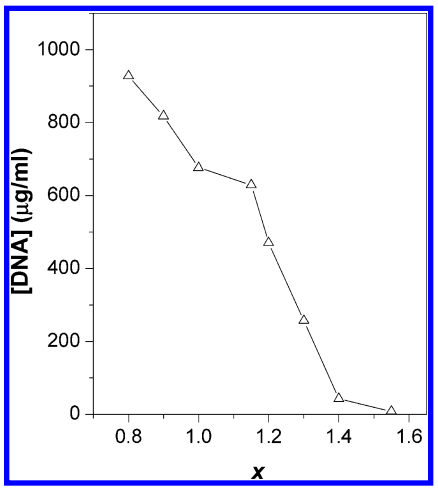


**Figure 8.** Concentration of DNA remained in the supernatant after the complexsation reaction for the complex with $m = 3$. The DNA concentration was determined from the absorbance at 260 nm in the UV−vis spectra. The DNA concentration is seen to decrease with increasing $x$.

in the bulk solution will shift the $L_\alpha^c$-to-$H_{II}^c$ transition to a higher temperature due to a lower entropic gain from the phase transition.

The concentration of uncomplexed DNA in the bulk solution was evaluated by measuring the concentration of DNA remaining in the supernatant after complexation using UV−vis spectroscopy. Figure 8 displays such a DNA concentration as a function of $x$ for the complex with $m = 3$. It can be seen that the concentration of DNA remaining in the bulk solution did decrease with increasing $x$. This is consistent with the higher $L_\alpha^c$-to-$H_{II}^c$ transition temperature observed at smaller $x$ due to lower entropic gain from counterion release.

## Conclusions

We have investigated the thermally-induced $L_\alpha^c$−$H_{II}^c$ transition of the complexes of polyanionic DNA with the cationic membranes consisting of a cationic surfactant, DTAB, and a neutral lipid, DOPE. The complexes formed $L_\alpha^c$ or $H_{II}^c$ structures depending on the membrane composition, charge ratio, and temperature. The SAXS profiles of the isoelectric complexes at room temperature indicated the formations of $L_\alpha^c$ and $H_{II}^c$ phases in the complex with $m = 3$ and 9, respectively. The electron density profiles associated with these two structures were constructed from the SAXS data to provide deeper insight into the structures formed. The effects of membrane composition and charge ratio on the thermotropic $L_\alpha^c$−$H_{II}^c$ transition have been revealed. $L_\alpha^c$−$H_{II}^c$ phase transition was not observable when the membrane consisted of relatively dilute amount of DOPE (e.g.,

(41) Wang, T. Y.; Lee, Y. R.; Sheng, Y. J.; Tsao, H. K. *J. Phys. Chem. B* **2005**, *109*, 22560.

$m = 1$). The order−order transition became accessible at $m \geq 2$ with the transition temperature decreasing with increasing DOPE content, since the DOPE, which by itself tended to organize into $H_{II}$ structure, promoted the formation of the columnar phase. We proposed that the transition from the $L_\alpha^c$ to $H_{II}^c$ phase was accompanied with the release of the counterions condensed on the phosphate groups not bound to DTAB in the $L_\alpha^c$ phase. The higher uncomplexed DNA concentration in the bulk solution at lower $x$ caused a lower entropic gain from such a counterion release and consequently raised the $L_\alpha^c$-to-$H_{II}^c$ transition temperature. Finally, from the X-ray scattering profiles in the high-$q$ region, DNA confined between the bilayers in the complexes was found to retain B conformation despite the electrostatic interaction with CS.

**Acknowledgment.** This work was supported by the Industrial Technology Research Institute, Taiwan, under Grant No. A331XS9E00. The synchrotron X-ray scattering experiment supported by the National Synchrotron Radiation Research Center (NSRRC) under Project ID 2004-3-047-5 was also gratefully acknowledged.

LA060862Z